55: Estimation of Snow Extent and Snow Properties

DOROTHY K HALL[1], RICHARD EJ KELLY[2], JAMES L FOSTER[1] AND ALFRED TC CHANG[1†]

[1]NASA/Goddard Space Flight Center, Greenbelt, MD, US
[2]University of Maryland, Baltimore, MD, US
[†]Deceased May 26, 2004

Important advances have been made in the measurement of seasonal snow cover since the advent of satellite remote sensing in the mid 1960s. Data from the visible, near-infrared, infrared, and microwave portions of the electromagnetic spectrum have proven useful for measuring different properties of snow. In terms of snow mapping, sensors employing visible and near-infrared wavelengths are now capable of accurately and reliably measuring snow-cover extent with a spatial resolution of up to 250 m on a daily basis, and even higher resolution for less-frequent coverage. Passive-microwave data, available since the 1970s, have been utilized for measuring snow extent, depth and snow-water equivalent (SWE), though at a coarse spatial resolution compared to visible data, while active-microwave sensors such as scatterometers, provide valuable information on snowpack ripening. Capabilities of synthetic-aperture radar (SAR) data for snow-cover studies are still being explored, however, bands on current satellite SAR sensors are not ideal for measuring snow cover. Remote sensing data of snow cover are now well suited for use in hydrologic and general-circulation models. Inclusion of remotely-sensed data significantly enhances our understanding of the Earth's weather and climate, and decadal-scale climate change. Future improvements include refinement of snow-cover extent measurements, minimizing SWE errors, and improving our ability to ingest remote sensing data of snow into models.

INTRODUCTION

Satellite remote-sensing technology has virtually revolutionized the study of snow cover. The high albedo of snow presents a good contrast with most other natural surfaces (except clouds), and therefore is easily detected by many satellite sensors. Weekly snow mapping of the Northern Hemisphere using National Oceanographic and Atmospheric Administration (NOAA) satellite data began in 1966 and continues today in the United States, but with improved resolution and on a daily basis (Matson *et al.*, 1986; Ramsay, 1998; Carroll *et al.*, 2001). In addition, using Earth Observing System (EOS) Moderate Resolution Imaging Spectroradiometer (MODIS) data, beginning in early 2000, global snow cover has been mapped on a daily basis at a spatial resolution of up to 500 m (Hall *et al.*, 2002a).

In addition to the visible/near-infrared data, from MODIS and NOAA satellite sensors, both passive and active microwave data have been useful for mapping snow and determining snow wetness and snow water equivalent (SWE) (Ulaby and Stiles, 1980) since the early 1970s. Using passive microwave data, snow extent, and SWE may be estimated globally on a daily basis since the launch of the Nimbus-7 Scanning Multichannel Microwave Radiometer (SMMR) (Chang *et al.*, 1987), and continuing with the May 2002 launch of the Advanced Microwave Scanning Radiometer (AMSR) (Kelly *et al.*, 2003). Active-microwave sensors, such as from the NASA scatterometer (NSCAT), are especially useful for detecting snowpack ripening (Nghiem and Tsai, 2001).

The geographical extent of snow cover over the Northern Hemisphere varies from a maximum of $\sim 46 \times 10^6$ km^2 in January and February to a minimum of $\sim 4 \times 10^6$ km^2 in

Encyclopedia of Hydrological Sciences. Edited by M G Anderson, 2005.

August; between 60 and 65% of winter snow cover is found over Eurasia, and most midsummer snow cover is in Greenland (Frei and Robinson, 1999). Numerous studies have shown the importance of accurate measurements of snow and ice parameters as they relate to the Earth's climate and climate change (for example, see Martinelli, 1979; Dewey and Heim, 1981 and 1983; Barry, 1983, 1984, and 1990; Dozier, 1987; Ledley *et al.*, 1999; Foster *et al.*, 1987 and 1996; Serreze *et al.*, 2000; Dozier and Painter, 2004). Measurements have become increasingly sophisticated over time. In addition, as the length of the satellite record increases, it becomes easier to determine trends that have climatic importance.

Three of the most important properties of a snow cover are depth, density, and water equivalent (Pomeroy and Gray, 1995). If the snow depth and density are known, then the SWE may be calculated. SWE is a hydrologically important parameter as it determines the amount of water that will be available as snowmelt.

After introducing snow as a medium, and reviewing its optical and microwave properties, we will show how remote sensing is used to study snow-covered area, SWE, snow wetness and snow albedo, and discuss the parameterization of snow in hydrologic and general circulation models (GCMs).

INTRODUCTION TO SNOW CRYSTALS AND DEVELOPMENT OF A SNOWPACK

Snow is a porous, permeable aggregate of ice grains (Bader, 1962). Snow crystals nucleate and begin their growth in clouds where the temperature is below 0 °C. Snow crystals can occur in a variety of relatively flat hexagonal or six-sided shapes (Figure 1), however, they can also occur as elongated columns and needles. Differences in snow crystals are a result of variations in the temperature and humidity of the atmosphere at the time of their formation and the action of the wind during their descent to the ground (Male, 1980). As a result, there is a myriad of possible shapes that can form depending primarily on the cloud temperature at the time the water vapor freezes.

Freshly fallen snow almost immediately begins to compact and metamorphose, initially preserving the original shape of the snow crystal. The constant jostling and rubbing of crystals against each other causes protuberances to become chipped and broken. As the snow settles under its own weight, melts and refreezes, and is buffeted by the wind, individual crystals are further altered such that after a few days they have little resemblance to their original shape. A seasonal snowpack might have grain radii ranging from 0.1 to 0.5 mm throughout the season.

In the absence of a temperature gradient in the snowpack, snowflakes undergo "destructive metamorphism" and become more rounded over time, with typically slower

Figure 1 This image of a newly fallen hexagonal plate snow crystal was taken with an Electron Scanning Microscope and shows a classic dendritic snow crystal, having a central hexagonal plate, but lacking sharp edges. Because of the air temperature at the time of collection (close to 0 °C), this crystal may have undergone some sublimation (Wergin *et al.,* 1996)

growth rates being more characteristic of the more-rounded crystals. "Constructive metamorphism," when large grains grow at the expense of small grains, occurs when there is a thermal and vapor gradient in the snowpack and snow grains at the base of the pack grow at the expense of smaller grains, hence the crystals develop distinctive shapes (Colbeck, 1982). Faster growth rates give rise to the faceted crystals. Dry snow will metamorphose into large depth-hoar grains when subjected to a strong temperature gradient, and grain growth and dry-snow metamorphism control the movement and redistribution of mass, chemical species, and isotopes in the snowpack (Sturm and Benson, 1997). Depth-hoar crystals may grow to 1 cm in size (Trabant and Benson, 1972).

Seasonal snowpacks develop from a series of winter storms and are often created by various forms of precipitation such as rain and freezing rain. Diurnal melting and refreezing, and wind action are also important in the ultimate development of a snowpack. Thus, seasonal snow cover usually develops a layered structure in which ice layers alternate with layers of a coarser texture (Male, 1980).

FUNDAMENTALS OF THE REMOTE SENSING OF SNOW

Introduction With optical remote sensing, there is a potential to determine the extent and albedo of a snow cover, and some inference as to snow depth can be made based on the ability of a snow cover to cover existing vegetation of known height. Infrared sensors can provide snow

surface temperature, which may be a useful parameter for hydrologic modeling. Microwave measurements have the capability to respond to the bulk properties of a snowpack as well as to variations in other surface and subsurface features because microwaves can penetrate the snowpack and thus provide information on snow depth and SWE when the snowpack is dry. Additionally, the microwave part of the spectrum allows remote observation of snow cover under nearly all weather and lighting conditions. SWE is of critical importance for water resources and hydrologic and GCM modeling. In short, use of optical, infrared, and microwave sensors provides synergy that allows extraction of important snowpack properties for use in models.

Optical Properties The spectral albedo of a surface is the upflux divided by the downflux at a particular wavelength (Warren, 1982). The spectral albedo of fresh snow in the visible region of the spectrum remains high but decreases slowly as snow ages, but in the near-infrared, the spectral albedo of aging snow decreases considerably as compared to fresh snow (O'Brien and Munis, 1975; Warren and Wiscombe, 1980; Wiscombe and Warren, 1980).

The broadband albedo is the reflectance across the reflective part of the solar spectrum. Broadband albedo decreases when grain size increases as the snow ages (Choudhury and Chang, 1979), and melting causes snow grains to grow and bond into clusters (Dozier *et al.*, 1981; Grenfell *et al.*, 1981; Warren, 1982). Snow albedo may decrease by $>25\%$ within just a few days as grain growth proceeds (Nolin and Liang, 2000). For example, Gerland *et al.* (1999) measured a maximum albedo $>90\%$ on Svalbard, Norway, before melt onset, and $\sim 60\%$ after melt had progressed in the spring when the snow was considered old, but still clean. The albedo of a snow cover is also influenced by the albedo of the land cover that it overlies, especially when the snowpack is thin.

Grain size may be estimated using remotely sensed data (Dozier, 1984; Nolin and Dozier, 1993). With the onset of surface melting and associated grain size increase, the near-infrared reflectance decreases dramatically (Warren, 1982) (Figure 2). The near-infrared albedo of snow is very sensitive to snow-grain size while visible albedo is less sensitive to grain size, but is affected by snow impurities. Modeling by Warren and Wiscombe (1980) demonstrates that small but highly absorbing particles can lower the snow albedo in the visible part of the spectrum by 5–15% compared to pure snow. Hansen and Nazarenko (2004) report that anthropogenic soot emissions have reduced snow and ice albedos by 3% in Northern Hemisphere land areas to yield a climate forcing of $+0.3\,\mathrm{W\,m^{-2}}$ in the Northern Hemisphere, thus contributing to global warming.

Though the reflectance of freshly fallen snow is nearly isotropic (Dirmhirn and Eaton, 1975), as snow ages, the specular reflection component increases, especially in the forward direction and with solar zenith angle (SZA) (Salomonson and Marlatt, 1968), and the anisotropic nature of snow reflectance increases with increasing grain size

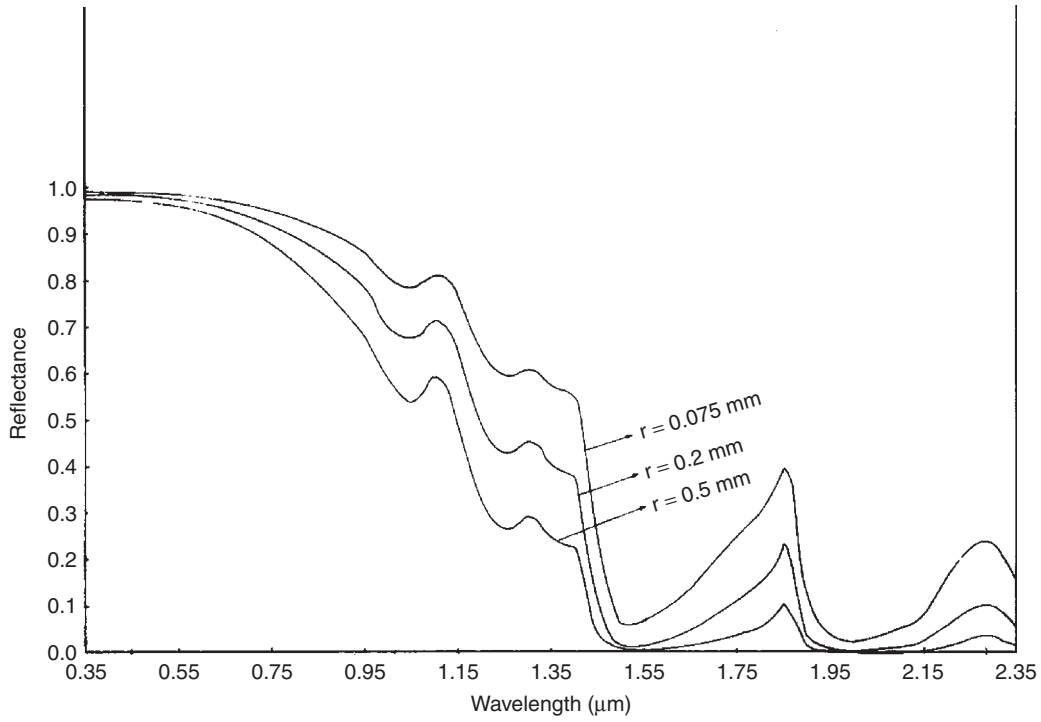

Figure 2 Illustration of the effect of different snow crystals on snow reflectance (From Choudhury and Chang, 1979)

(Steffen, 1987). Effective snow-grain radii typically range in size from ~50 μm for new snow, to 1 mm for wet snow consisting of clusters of ice grains (Warren, 1982).

Snow albedo increases at all wavelengths with the SZA. Additionally, cloud cover normally causes an increase in spectrally integrated snow albedo due to multiple reflections caused by clouds (Grenfell and Maykut, 1977; Warren, 1982).

Microwave Properties In the microwave part of the spectrum (300 to 1 GHz, or 1 mm to 30 cm wavelength), remote sensing can be accomplished either by measuring emitted radiation with a radiometer or by measuring the intensity of the return (in decibels) of a signal sent by a radar.

Microwave emission from a layer of snow over a ground surface consists of contributions from the snow itself and from the underlying ground. Both contributions are governed by the transmission and reflection properties of the air-snow and snow-ground interfaces, and by the absorption/emission and scattering properties of the snow layer.

The dielectric properties of snow at a given microwave frequency are generally dependent on the relative proportion of liquid and solid water in the snow by volume. Even at temperatures <0 °C, liquid-like water exists in thin films surrounding, and bound to, ice crystals (Hobbs, 1974), but is considered to be dry since it contains no "free" liquid water (Leconte *et al.*, 1990). However, snow that contains a large amount of liquid water (>5% by volume) has a high dielectric constant (>35 below 20 GHz) relative to that of dry snow.

Theoretically, the dielectric constant of snow consists of the sum of a real and an imaginary part. Snow is a mixture of air and ice, the dielectric constant of air being 1.0 and ice 3.17 ± 0.07 for frequencies from 1 MHz to well above the microwave region (Evans, 1965). Snow has a dielectric constant between l.2 and 2.0 when the snow densities range from 0.1 to 0.5 g cm^{-3} (Hallikainen and Ulaby, 1986).

If a dry snowpack contains ice and snow layers, specular reflection at the interfaces between layers may occur resulting in strongly enhanced backscatter in the case of active-microwave remote sensing (Mätzler and Schanda, 1984). Or, if the grain sizes of a dry snowpack are large enough relative to the microwave wavelength, volume scattering will occur. Otherwise, the signal is returned mainly from the ground/snow interface.

Longer wavelengths, in general, travel almost unaffected through dry snow. X-band (2.4–3.75 cm, 8.0–12.5 GHz) or lower frequencies (longer wavelengths) are not generally useful for detecting and mapping thin, dry snow because the size of snow particles is much smaller than the size of the wavelength. Thus, at these longer wavelengths, there is little chance for a microwave signal to be attenuated and scattered by the relatively small ice crystals comprising a snowpack (Waite and MacDonald, 1970; Ulaby and Stiles, 1980, 1981). Wavelengths longer than ~10–15 cm are not impeded as they move through most dry seasonal snowpacks (Bernier, 1987).

For snow crystals of a radius >~0.1 mm, scattering dominates emission at higher (>15 GHz) microwave frequencies (Ulaby *et al.*, 1986). Absorption is determined primarily by the imaginary part of the refractive index. In dry snow, the imaginary part is very small, several orders of magnitude smaller than for water (Ulaby and Stiles, 1980).

The backscatter received by a synthetic-aperture radar (SAR) antenna is the sum of surface scattering at the air/snow interface, volume scattering within the snowpack, scattering at the snow/soil interface, and volumetric scattering from the underlying surface (if applicable). Most techniques developed for mapping snow cover using SAR data show promise for mapping only wet snow (see, for example, Rott and Nagler, 1993; Shi *et al.*, 1994). This is because it is difficult to distinguish dry snow from bare ground using SAR data at the X-band and lower frequencies that are currently flown in space. Volume scattering from a shallow, dry snow cover (SWE <20 cm) is undetectable at C-band (5.3 GHz, 5.6 cm), for example, because the backscatter is dominated by soil/snow scattering. Volume-scattering in dry snow results from scattering at dielectric discontinuities created by the differences in electrical properties of ice crystals and air, and by ice lenses and layers. Atmospheric scattering is usually very small and can be neglected (Ulaby and Stiles, 1980; Leconte *et al.*, 1990; Leconte, 1995).

In the case of wet snow (Stiles and Ulaby, 1980; Ulaby and Stiles, 1980; Rott, 1984; Ulaby *et al.*, 1986), when at least one layer of the snowpack (within the penetration depth of the radar signal) becomes wet (4–5% liquid water content), the penetration depth of the radar signal is reduced to about 3–4 cm (or one wavelength at X-band) (Mätzler and Schanda, 1984). Thus, there may be high contrast between snow-free ground and ground covered with wet snow, thus making it possible to distinguish wet and dry land or snow when imaged with C-band SAR from space.

Volume scattering increases with snow-grain size and internal layering, and with amount of snow. Radiation at wavelengths comparable in size to the snow crystal size (about 0.05–3.0 mm, or greater if depth hoar is present) is scattered in a dry snowpack according to Mie scattering theory. (Mie scattering predominates when the particles causing the scattering are larger than the wavelengths of radiation in contact with them.) Currently, only passive microwave sensors operate at these wavelengths from satellites.

In the microwave part of the spectrum, the radiation emitted from a perfect emitter is proportional to its physical temperature, T. However, most real objects emit only a fraction of the radiation that a perfect emitter would emit at its physical temperature. The equivalent temperature of

the microwave radiation thermally emitted by an object is called its *brightness temperature*, T_B, expressed in Kelvins. This fraction defines the emissivity, E, of an object (Chang *et al.*, 1976). In the microwave region,

$$E = \frac{T_B}{T} \tag{1}$$

Microwave emission from a layer of snow over a ground medium consists of two contributions: (i) emission by the snow volume and (ii) emission by the underlying ground. Both contributions are governed by the transmission and reflection properties of the air-snow and snow-ground interfaces, and by the absorption/emission and scattering properties of the snow layer (Stiles *et al.*, 1981), and a myriad of physical parameters that affects the emission (Derksen *et al.*, 2002). As an electromagnetic wave emitted from the underlying surface propagates through a snowpack, it is scattered by the randomly spaced snow particles in all directions. As the snowpack grows deeper, there is more loss of radiation due to scattering, and the emission of the snowpack is reduced, thus lowering the T_B. The deeper the snow, the more crystals are available to scatter the upwelling microwave energy, and, thus, it is possible to estimate the depth and water equivalent of the snow using passive-microwave remote sensing.

Snow grains scatter the electromagnetic radiation incoherently and are assumed to be spherical and randomly spaced within the snowpack. Although most snow particles are generally not spherical in shape, using Mie theory, their optical properties can be simulated as spheres (Chang *et al.*, 1976). We will discuss the scattering power of a variety of different snow crystal shapes and their effect on the microwave emission of a snowpack in a later section.

A wet snowpack radiates like a blackbody at the physical temperature of the snow layer, and is therefore indistinguishable from snow-free soil using microwave remote sensing (Kunzi *et al.*, 1982). The dielectric constants of water, ice, and snow are different enough so that even a little surface melting causes a strong microwave response (Schanda *et al.*, 1983; Foster *et al.*, 1987). The scattering loss decreases drastically with increasing liquid water content (free water) and becomes negligible for values above about 1% (Hallikainen, 1984).

SNOW MAPPING

Early attempts to forecast runoff from the areal extent of snow cover used terrestrial photographs (Potts, 1937). Other observations from aircraft were also undertaken such as locating and mapping snow-cover extent and mapping the location of the snowline. Along with volume, the areal extent of snow cover has been used to predict snowmelt runoff and to forecast floods.

Because of its high albedo, snow was easily observed in the first image obtained from the Television Infrared Operational Satellite-1 (TIROS-1) weather satellite in 1960. Data from meteorological satellites and manned spacecraft were useful in determining snowline elevation, delineating snow boundaries, and observing changes in snow conditions due to rising temperatures and rain-on-snow events (Singer and Popham, 1963), and later, seasonal streamflow could also be estimated (Rango and Salomonson, 1977). Data from Environmental Science Services Administration (ESSA) operational satellites were used as early as the mid-to-late 1960s to determine areal extent of snow cover.

A major step forward in snow mapping came with the advent of the Landsat series of sensors beginning in 1972. Landsat-1 carried a Multispectral Scanner (MSS) sensor with 80-m spatial resolution. With Landsat data came the ability to create detailed basin-scale snow-cover maps on a regular basis when cloudcover permitted. At first, the repeat-pass interval for the Landsat satellite was 18 days, but this was decreased to 16 days with the launch of Landsat-4 in 1982. Landsats-4 and -5 carried a Thematic Mapper (TM) sensor with 30-m resolution, and Landsat-7 carries an Enhanced Thematic Mapper Plus (ETM+) with spatial resolution of 30 m, except in the panchromatic band where the resolution is 15 m. As of this writing, the TM onboard the Landsat-5 satellite is still operating. (Landsat-6 was lost after it failed to reach orbit in 1993.) Though the Landsat series has provided high-quality, scene-based snow maps, the 16- or 18-day repeat-pass interval of the Landsat satellites is not adequate for most snow-mapping requirements, especially during spring snowmelt.

Operational Snow-cover Mapping in the United States The NOAA National Environmental Satellite, Data, and Information Service (NESDIS) began to generate Northern Hemisphere Weekly Snow and Ice Cover analysis charts derived from NOAA's Geostationary Operational Environmental Satellite (GOES) and Polar Orbiting Environmental Satellite (POES) visible satellite imagers in November 1966. Maps were manually constructed, and the spatial resolution of the charts was 190 km. Since 1997, the Interactive Multi-sensor Snow and Ice Mapping System (IMS) has been used by analysts to produce products daily at a spatial resolution of about 25 km, and utilizes a variety of satellite data to generate the maps (Ramsay, 1998). This snow-cover record has been studied carefully (Robinson *et al.*, 1993; Robinson, 1997, 1999) and has been reconstructed following adjustment for inconsistencies that were discovered in the early part of the data set (Robinson and Frei, 2000; Frei *et al.*, 1999). Results show that the Northern Hemisphere annual snow-covered area has decreased (Robinson *et al.*, 1993; Brown and Goodison, 1996; Hughes and Robinson, 1996; Hughes *et al.*, 1996; Armstrong and Brodzik, 1998, 2001; Frei *et al.*, 1999;

Brown, 2000); satellite data show a decrease of about 0.2% per year from 1979–1999 (Armstrong and Brodzik, 2001).

The National Operational Hydrologic Remote Sensing Center (NOHRSC) snow-cover maps, generated by National Weather Service NOHRSC hydrologists, are distributed electronically in near real time to local, state, and federal users during the snow season (Carroll, 1987 and 1995; Cline *et al.*, 1998; Carroll *et al.*, 2001). The NOHRSC 1-km maps are generated primarily from the NOAA polar-orbiting satellites and GOES satellites to develop daily digital maps depicting the areal extent of snow cover for the coterminous United States and Alaska, and parts of southern Canada.

Other Snow Maps Landsat data have been used for measurement of snow-covered area over drainage basins (Rango and Martinec, 1979, 1982). The Landsat TM and ETM+ have been especially useful for measuring snow cover because of the short-wave infrared band – band 6(1.6 μm), which allows snow/cloud discrimination. The reflectance of snow is low and the reflectance of most clouds remains high in that part of the spectrum. Various techniques, ranging from visual interpretation, multispectral image classification, decision trees, change detection, and ratios (Kyle *et al.*, 1978; Bunting and d'Entremont, 1982; Crane and Anderson, 1984; Dozier, 1989; Romanov *et al.*, 2000; Hall *et al.*, 2002a; Romanov and Tarpley, 2003) have been used to map snow cover. Other spectral and threshold tests are also used.

The MODIS was first launched in December 1999 on the Terra spacecraft. MODIS data are now being used to produce daily and eight-day composite (Figure 3) snow-cover products from automated algorithms **http://modis-snow-ice.gsfc.nasa.gov** at Goddard Space Flight Center in Greenbelt, Maryland (Hall *et al.*, 2002a). The products are transferred to the National Snow and Ice Data Center (NSIDC) in Boulder, Colorado, where they are archived and distributed via the Earth Observing System Data Gateway (EDG) **http://nsidc.org** (Scharfen *et al.*, 2000). The Aqua satellite was launched in 2002 with a second MODIS instrument that enables snow-covered area measurements to be extended farther into the future (Riggs and Hall, 2004).

The MODIS maps provide global, daily coverage at 500-m resolution, and the climate-modeling grid (CMG) maps are available at 0.05 °resolution, which is ~5.6 km at the Equator. The CMG map, designed for climate modelers, provides a global view of the Earth's snow cover in a geographical projection with fractional snow cover reported in each cell. The automated MODIS snow mapping algorithm uses at-satellite reflectances in MODIS bands 4 (0.545–0.565 μm) and 6 (1.628–1.652 μm) to calculate the normalized difference snow index (NDSI) (Hall *et al.*, 2002a). Other threshold tests are also used, including the Normalized Difference Vegetation Index (NDVI) together with the NDSI to improve snow mapping in forests (Klein *et al.*, 1998). Mauer *et al.* (2003) compared MODIS and NOHRSC data for the Columbia River Basin, USA, and found that the maps were comparable, but the MODIS maps generally provided more cloud-free data than did the NOHRSC maps. Other studies have also shown the MODIS snow maps to represent an advance in global snow mapping.

Fractional Snow Cover or Subpixel Snow Mapping Fractional snow cover (FSC) utilizing Landsat and MODIS data has been derived to exploit subpixel information. Much of this work has relied on spectral-mixture modeling (see Nolin *et al.*, 1993; Rosenthal and Dozier, 1996; Vikhamer and Solberg, 2002; Dozier and Painter, 2004), and neural networks (Simpson and McIntire, 2001) but does not provide global coverage. Painter *et al.* (2003) couple

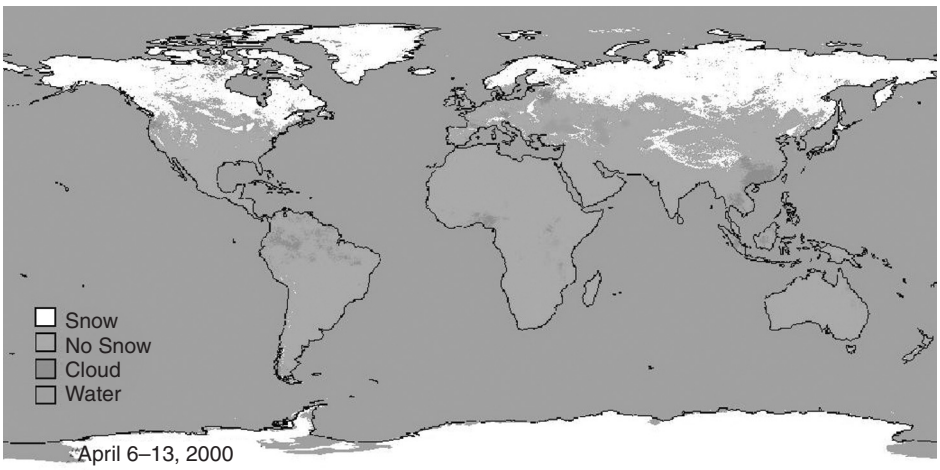

Figure 3 MODIS 8-day composite CMG global snow-cover map. A color version of this image is available at http://www.mrw.interscience.wiley.com/ehs

spectral-mixture analysis with a radiative transfer model to retrieve subpixel snow-covered area and effective grain size from Airborne Visible/Infrared Imaging Spectrometer (AVIRIS) data.

Recently, Salomonson and Appel (2004) have extended the use of the NDSI to provide FSC globally with absolute errors of 0.1 or less over the whole range of FSC from 0 to 100%. In the near future, percent snow cover or fractional snow cover in each pixel (Salomonson and Appel, 2004) will be provided in the 500-m products. Other work using MODIS data (Kaufman *et al.*, 2002) has also developed algorithms to map FSC globally.

The Norwegian Water Resources and Energy Directorate (NVE) and the Tromso Satellite Station (TSS) produce snow maps from Advanced Very High Resolution Radiometer (AVHRR) data using band 2 (0.7–1.1 μm) for snow mapping, and bands 3 (3.6–3.9 μm), 4 (10.3–11.3 μm), and 5 (11.5–12.5 μm) for snow/cloud discrimination (Anderson, 1982; König *et al.*, 2001). An upper limit of 100% snow cover is determined from a glacier or 100% snow-covered region and a lower limit of 0% is determined from water or land areas, and percentage of snow cover is interpolated linearly, thus deriving FSC (König *et al.*, 2001).

Snow Mapping Using Microwave Sensors For dry snow, the naturally emitted microwave radiation of a snowpack is related to several physical properties of the snow as discussed earlier. These properties include the number of snow grains along the emission path (the snow depth in cm), the size of grains (grain radius in mm), and the packing of the grains (volume fraction in % or density in $\mathrm{kg\,m^{-3}}$). Such components control the propagation of radiation, especially at higher frequencies (e.g. 36 GHz) but affect the microwave response less at lower frequencies (e.g. 18 GHz). The brightness temperature difference between 18 GHz and 36 GHz ($T_B18 - T_B36$) is used to minimize the effect of snow temperature on the microwave emissivity. This is the principle that has been used to estimate SWE and snow depth from passive microwave instruments (Chang *et al.*, 1976, 1982; Kunzi *et al.*, 1976, 1982; Goodison and Walker, 1994; Goodison *et al.*, 1986; Grody and Basist, 1996; Foster *et al.*, 1997; Kelly and Chang, 2003). Experiments and applications have shown that:

$$SD = a(T_B18\mathrm{H} - T_B36\mathrm{H}) \qquad (2)$$

where SD is the snow depth in cm, a is constant of 1.59 for SMMR and is derived from radiative transfer experiments (Chang *et al.*, 1982), and $T_B18\mathrm{H}$ and $T_B36\mathrm{H}$ are the horizontally polarized brightness temperatures measured by the spacecraft at 18 and 36 GHz, respectively. If SWE is desired, a is set to a value of 4.8. Research into estimation of SWE and snow depth from passive microwave instruments has used this principle and an example of its application to AMSR-E data is shown in Figure 4 (Kelly *et al.*, 2003).

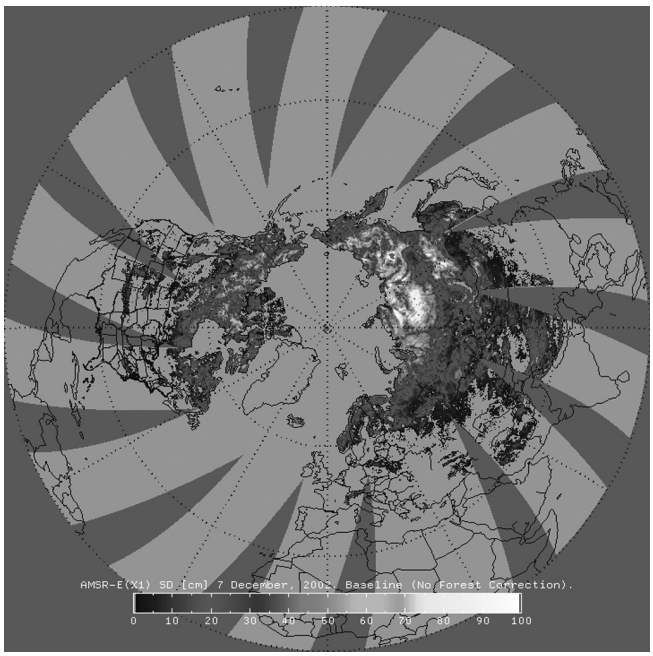

Figure 4 Estimated snow depth for the Northern Hemisphere from AMSR-E data for 7 December 2002 (From R.E.J. Kelly and A.T.C. Chang, unpublished data). A color version of this image is available at http://www.mrw.interscience.wiley.com/ehs

Rott and Nagler (1995) developed a threshold-based algorithm to map the extent of melting snow areas in mountainous regions on glaciers using ERS-1 SAR data. The classification is based on the ratio of the backscatter of the image with wet snow cover *versus* the backscatter of the reference image. They determined a threshold value of −3 dB by comparison with field observations. Using a single-layer backscatter model, seasonal variations as well as day/night changes in snow-covered alpine areas are shown by Nagler and Rott (2000) to be largely due to changes of the liquid water content of the snowpack and the snow surface roughness. They showed the same threshold of −3 dB for identifying wet snow using C-band HH Radarsat SAR and C-band ERS SAR data. Comparison of SAR-derived snow maps with Landsat-derived snow maps showed generally good results, but with a systematic underestimation of the snow extent at the edges of the snowpack using the SAR data.

In alpine regions, Shi *et al.* (1994) used single-pass SAR imagery with polarization to map wet snow cover, finding it difficult to distinguish dry snow cover from bare ground and short vegetation. Further work using single-pass, multifrequency (SIR-C/X-SAR) data (Shi and Dozier, 1997) showed that the coherence between two passes provides a useful measurement and allows development of

algorithms to map both wet and dry snow under specific circumstances.

MODIS snow maps were compared with SSM/I-derived snow maps over the prairie and boreal forest region in western Canada by Bussières *et al.* (2002); generally good correspondence was found in the taiga region in eastern Canada, however, the accuracy of the SSM/I maps was reduced in the fall and spring. As the snow deepens during the winter, snow-grain sizes increase and the temperatures become consistently colder, the ability of the SSM/I to map snow improves, and the agreement between the visible and passive microwave maps improves (Basist *et al.*, 1996). This is because the passive microwave data are not able to effectively map wet snow cover since the penetration of the microwave signal upward through the snowpack is extremely low when the snow is wet.

Snow Albedo

Early attempts to measure snow albedo remotely were conducted from aircraft (Bauer and Dutton, 1962; Hanson and Viebrock, 1964; McFadden and Ragotzkie, 1967; Salomonson and Marlatt, 1968; Dirmhirn and Eaton, 1975). More recently, however, detailed field, aircraft, and satellite studies have been undertaken to derive quantitative measurements of snow reflectance and albedo (for example, see Steffen, 1987; Hall *et al.*, 1989; Duguay and LeDrew, 1992; Winther, 1993; Knap and Oerlemans, 1996; Stroeve *et al.*, 1997; Winther *et al.*, 1999; Greuell *et al.*, 2002).

Some researchers have measured the albedo of snow-covered lands using satellite data on a hemispheric scale (e.g. Kukla and Robinson, 1980; Robock, 1980; Robinson and Kukla, 1985; Robinson *et al.*, 1992; Robinson, 1993). Both Robinson *et al.* (1986) and Scharfen *et al.* (1987) constructed basinwide albedo maps and observed differences in the timing of the melt between years. Robinson and Kukla (1985) used Defense Meteorological Satellite Program (DMSP) imagery (spectral range – 0.4–1.1 μm) to derive a linear relationship between the brightest snow-covered arctic tundra and the darkest snow-covered forest, which were assigned albedos of 0.80 and 0.18, respectively. Scene brightness was then converted to surface albedo by linear interpolation. The surface brightness is a function of the type and density of vegetation and the depth and age of snow (Robinson and Kukla, 1985). The derived "maximum" surface albedo values were useful for climate modeling (Ross and Walsh, 1987).

Surface albedo has also been derived from Landsat MSS and TM data. One approach, based on exact solutions of the radiative transfer equation for upwelling intensity, requires known albedo values derived in each Landsat scene at different points (Mekler and Joseph, 1983). Other approaches rely on a narrowband to broadband conversion to derive albedo (Brest and Goward, 1987; Hall *et al.*, 1989; Duguay and LeDrew, 1992; Knap *et al.*, 1998; Winther *et al.*, 1999). Knap and Reijmer (1998) used Landsat data to derive the Bidirectional Reflectance Distribution Function (BRDF) to describe the complete distribution of the anisotropic reflectance of snow, and Greuell and de Ruyter de Wildt (1999) used BRDF to correct for anisotropic reflectance. The BRDF is the physical property that determines the amount and angular distribution of reflected radiance from a surface (Nicodemus *et al.*, 1977).

AVHRR data have been used to map changes in albedo over the Greenland Ice Sheet during the spring and summer months (Knap and Oerlemans, 1996; Nolin and Stroeve, 1997; Stroeve *et al.*, 1997). While Stroeve *et al.* (1997) found a good correspondence with satellite-derived and surface-measured albedo before snowmelt, after snowmelt began, melt-water ponding on the ice surface precluded accurate comparisons between the satellite-derived and surface-measured albedo.

A near-surface global algorithm has been developed to map snow albedo using MODIS data (Klein and Stroeve, 2002). In deriving albedo, atmospherically corrected MODIS surface reflectances in individual MODIS bands for snow-covered pixels located in nonforested areas are adjusted for anisotropic scattering effects using a discrete ordinates radiative transfer (DISORT) model and snow optical properties. Currently, in the algorithm, snow-covered forests are considered to be Lambertian reflectors. The adjusted spectral albedos are then combined into a broadband albedo measurement using a narrow-to-broadband conversion scheme developed specifically for snow by Shunlin Liang (written communication, 2003) (Liang, 2000; Klein and Stroeve, 2002). A near-global snow albedo product (Figure 5) is available from February 2000 to the present and validation of this product is ongoing.

Snow-water Equivalent

To derive the SWE using passive microwave data, a radiative transfer approach is used in which, for example,

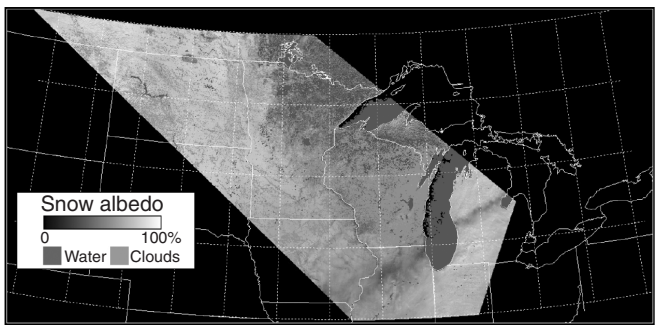

Figure 5 MODIS snow albedo product – north central United States and southern Canada – February 16, 2001. A color version of this image is available at http://www.mrw.interscience.wiley.com/ehs

an average crystal size of 0.3 mm (radius), a density of 300 kg m^{-1}, and a spherical shape are assumed. It is also assumed that the crystals scatter radiation incoherently and independently of the path length between scattering centers. These quantities are then used in radiative transfer equations to solve the energy transfer through the snowpack (Chang *et al.*, 1976, 1987). Equations 1 and 2 are derived from this work and reasonable results are obtained from its implementation. However, if the crystal radii and snow density differ significantly from the averages and assumptions, then poor SWE values may result. Current efforts are aimed at improving the methods to estimate SWE by incorporating more dynamic parameterizations of these variables.

When viewed with an electron microscope, the detail is so great that individual crystals (Figure 1) can be assigned a specific shape, but the variation between even adjacent crystals can be substantial (Rango *et al.*, 1996; Wergin *et al.*, 2002). While crystal size and effective crystal size (Mätzler, 1997) are strongly related to microwave brightness temperature, it appears from modeling results that the shape of the snow crystal is of little consequence in accounting for the transfer of microwave radiation (at least at 0.81 cm) from the ground through the snowpack (Foster *et al.*, 1999, 2000; Tsang *et al.*, 2000).

Currently, SWE of a dry snowpack can be estimated with passive microwave sensors such as the SSM/I, and the AMSR (see Table 1), which was launched on the Aqua satellite in May of 2002. In Canada, SSM/I data are used to provide operational SWE map products (Figure 6) for the Canadian prairie region.

Forest cover can adversely affect the SWE retrieval accuracy by reducing the characteristic scattering response from snow by suppressing the $T_B18\mathrm{H} - T_B36\mathrm{H}$ signal (Tiuri and Hallikainen, 1981; Hall *et al.*, 1982; Hallikainen, 1984; Kurvonen and Hallikainen, 1997). Foster *et al.* (1997) attempted to correct for this effect by incorporating forest fraction into equation (1) such that:

$$SD = \frac{a(T_B18\mathrm{H} - T_B36\mathrm{H})}{(1-ff)} \qquad (3)$$

where *ff* is the per pixel forest fraction (expressed as a unit percent) that ranges from 0% to 50% (fractions greater than 50% are set to 50%). This approach improved the retrieval accuracy in forested regions.

Snow-grain size is another important parameter that influences the microwave brightness temperature. A model was developed to study the growth of the depth-hoar layer at the base of the snowpack on the Arctic Coastal Plain of Alaska during winter and compared to brightness temperature as derived from the SMMR by Hall *et al.* (1986). Results showed that an approximately 20 K lower T_B was found at inland sites with a comparable snow depth, but a thicker depth-hoar layer than was present at coastal sites. Thus, it is necessary to characterize snow-grain size on a regional basis to enhance the accuracy of snow retrievals using passive microwave data. Using SSM/I data, Mognard and Josberger (2002) modeled seasonal changes in snow grain size using a temperature gradient approach. This information was then used to parameterize the retrieval of snow depth in the northern Great Plains during the 1996–1997 winter season. Taking this approach further, Kelly *et al.* (2003) have recently developed a methodology to estimate snow-grain size and density as the snowpack evolves through the season using SSM/I and simple statistical growth models. These estimated variables are then coupled with a dense media radiative transfer (DMRT) model, described in Tsang and Kong (2001) and Chang *et al.* (2003), to estimate SWE.

As early as 1972, Meier (1972) was able to map the snowline on Mt. Rainier in Washington State in the US, using the 270 K-T_B line and a single channel (19.35 GHz) of an airborne radiometer. Since then, many different algorithms to map snow cover and SWE using passive microwave data have been developed and tested (e.g. Rott *et al.*, 1981; Kunzi *et al.*, 1982; Chang *et al.*, 1982; Goodison, 1989; Goodison and Walker, 1994; Mätzler, 1987; Hallikainen and Jolma, 1992; Grody and Basist, 1996 and Derksen *et al.*, 2002; Pivot *et al.*, 2002; Walker *et al.*, 2002). Some appear to work better under certain conditions than others, and it is now well accepted that there is no algorithm that is ideal globally.

Table 1 Comparison of characteristics of passive microwave sensors (from Foster *et al.*, 2005)

	SMMR	SSM/I	AMSR-E
Platform	Nimbus-7	DMSP F-8, 11, 13	Aqua
Period of Operation	1979–87	1987 to present	2002 to present
Data Acquisition	every other day	daily	daily
Swath Width	780 km	1400 km	1600 km
Frequency (GHz)	18.0 37.0	19.35 37.0	18.7 36.5
Spatial Resolution (km)	60 × 40 (18 GHz) 30 × 20 (37 GHz)	69 × 43 (19.4 GHz) 37 × 29 (37 GHz)	28 × 16 (19.7 GHz) 14 × 8 (36.5 GHz)
Polarization	H & V	H & V	H & V
Orbital Timing (equation Crossing) (for minimum temperature)	midnight	6:00 a.m.	1:30 a.m.

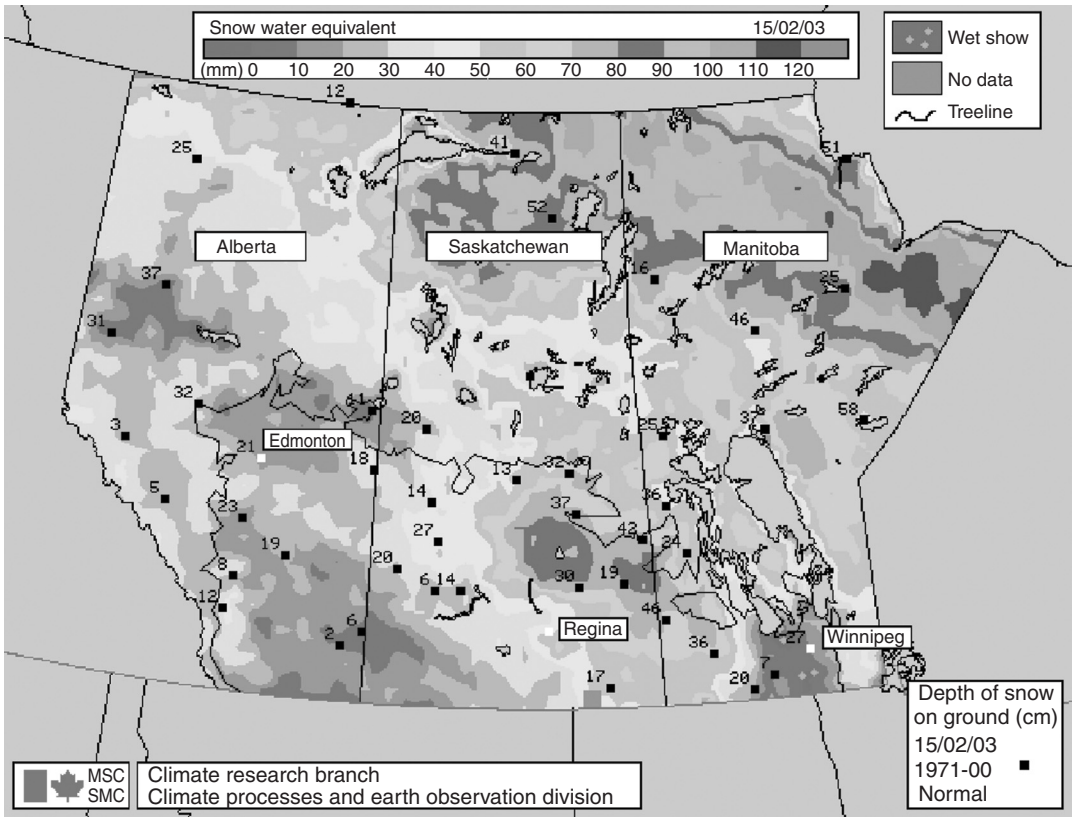

Figure 6 Snow water equivalent (in mm) over the Canadian Prairie region, derived from DMSP SSM/I data for 15 February, 2003. Areas of highest snow water equivalent generally correspond to the areas where the snow cover is deepest (Courtesy of the Climate Research Branch, Meteorological Service of Canada, Environment Canada). A color version of this image is available at http://www.mrw.interscience.wiley.com/ehs

The basic algorithm must be tuned to individual land-cover types (Walker and Goodison, 2000). Walker and Goodison (1993) developed a wet snow indicator using the SSM/I 37 GHz polarization difference for the Canadian Prairies, and Goita *et al.* (2003) developed separate algorithms, both based on the vertically polarized difference index using 18 and 37 GHz data from SSM/I to map SWE in deciduous and coniferous forest types, respectively.

The differences between the day and night brightness temperatures indicate the presence of liquid water in the snowpack. Early in the snow season, the difference is small, indicating the absence of liquid water in the snowpack. As spring approaches, the difference increases, indicating the presence of liquid water during the day, and then the pack refreezes at night. When liquid water does not refreeze at night, the difference again becomes small, and the snowpack is ripe and will soon begin to melt (Josberger *et al.*, 1993). Ramage and Isacks (2002) used SSM/I-derived diurnal-amplitude variations to detect early melt on snow-covered icefields in southeast Alaska, and found that melt timing correlates well with nearby stream hydrographs.

Climate-data-record (CDR) quality data sets of SWE are difficult to derive. The development of long-term CDR quality datasets may be influenced by difficulties related to calibration between sensors. Derksen *et al.* (2003) produced a time series for central North America for the winter season from 1978 through 1999, using both SMMR and SSM/I data. They found evidence of systematic SWE underestimation during the SMMR years, and overestimation of SWE during the SSM/I years. Previous work by Armstrong and Brodzik (2001) also suggested inconsistencies between the SMMR and SSM/I datasets.

Many other researchers have developed algorithms that use multiple sensors to map snow cover and SWE (e.g. Basist *et al.*, 1996; Armstrong and Brodzik, 1998, 2001, 2002; Standley and Barrett, 1999; Tait *et al.*, 2000 and, 2001; Kelly, 2001; Hall *et al.*, 2002b), and in different land covers (Hall *et al.*, 2001). Visible/near-infrared data, with good spatial resolution, provide excellent snow-covered area determination under cloud-free conditions, while passive microwave data provide all-weather day/night snow maps, but with coarser resolution. In addition, problems arise in wet snow and thin, dry snow when using passive microwave data alone.

There are conflicting results showing the sensitivity of radars to SWE. Ulaby *et al.* (1977) found that radar

sensitivity to total SWE (for wet snow) increased in magnitude with increasing frequency (or shorter wavelength) and is almost independent of angle for angles of incidence $>30°$, particularly at higher frequencies. Goodison *et al.* (1980) found little or no relationship between radar return and snowpack properties under either wet or dry snow conditions using L-band airborne SAR. A uniform, low return was found for a given area under both snow-free and snow-covered conditions. However, using X-band, in their study area near Ottawa, Ontario, nonforested areas exhibited higher backscatter when snow cover was present. Areas of ice and dense snow were observed to produce relatively higher radar returns using the X-band SAR (Goodison *et al.*, 1980).

Bernier *et al.* (1999) established a relationship between the backscattering ratios of a winter (snow covered) image and a fall (snow-free) image to estimate the snowpack thermal resistance using the Radarsat SAR. They then estimated the SWE from the thermal resistance and the measured mean density. In related work, Gauthier *et al.* (2001) used Radarsat C-band ScanSAR data to derive SWE in the La Grande River Basin in northern Québec, where they found ScanSAR-derived SWE values to be similar ($\pm 12\%$) to those derived from *in situ* snow measurements in January and March 1999.

SNOW WETNESS

A study of wet snow using C-, L- (1.25 GHz), and P-band (440 MHz) (see Table 2) polarimetric SAR of a mountainous area in Austria (Otzal), Rott *et al.* (1992) showed the importance of surface roughness at C- and L-band frequencies, and the increasing importance of the snow volume contribution with the longer wavelength P-band sensor. Radar polarimetry allows simultaneous measurement of the radar backscatter from a given surface at a number of different polarizations. Using European Remote Sensing Satellite (ERS)-1 images acquired before, during and after the melt period, Koskinen *et al.* (1997) successfully mapped wet snow with C-band SAR in unforested and sparsely forested regions in northern Finland.

Table 2 Band designations, wavelength, and frequency ranges for Earth-sensing radars (Long, 1975)

Band	Wavelength range (cm)	Frequency range (GHz)
Ka-band	0.75–1.1	26.5–40.0
K-band	1.1–1.67	18.0–26.5
Ku-band	1.67–2.4	12.5–18.0
X-band	2.4–3.75	8.0–12.5
C-band	3.75–7.5	4.0–8.0
S-band	7.5–15.0	2.0–4.0
L-band	15.0–30.0	1.0–2.0
P-band	30.0–100.0	0.3–1.0

Extensive aircraft and ground measurements were obtained by the Canada Centre for Remote Sensing (CCRS) over agricultural areas in southern Québec, Canada, in 1988–1990 (Bernier and Fortin, 1998). It was concluded that, at C-band, volume scattering from a shallow dry snowpack (SWE <20 cm) is not detectable. The backscatter using a C-band SAR emanates from the snow/soil interface when the snowpack is dry. Earlier, Mätzler and Schanda (1984) and Mätzler (1987) had concluded that the backscatter change between an unfrozen bare soil and a dry snow cover over unfrozen soil was small – on the order of 1.5 dB at X-band. Rott and Mätzler (1987) found no significant difference between snow-free and dry-snow-covered regions at 10.4 GHz. However, there may be a potential for detecting shallow, dry snow cover with C-band SAR data when the soil beneath the snow is frozen (Bernier and Fortin, 1998).

Though the main scattering contribution from a dry snow cover is from the ground/snow interface, small changes in the snow can be detected using tandem pairs from repeat-pass interferometric synthetic-aperture radar (InSAR) data. Using the coherence measurement of repeat passes, Shi and Dozier (2000) found that both wet and dry snow can be mapped as evidenced by comparison of snow mapped using Landsat imagery. Refraction of microwaves in dry snow was shown to have a significant effect on the interferometric phase difference and a relationship between changes in SWE and the interferometric phase was derived. Using three tandem pairs of InSAR data, Guneriussen *et al.* (2001) found that a snow density of $0.2\,\mathrm{g\,cm^{-2}}$ at 23° incidence angle gives phase wrapping for changes in snow depth of 16.4 cm and equals a SWE of 3.3 cm.

A promising technology for measuring snow cover is scatterometry. A Ku-band (14.6 GHz) scatterometer operated for three months from July to September 1978 on the Seasat satellite, and results show that some of the glacier facies could be mapped using derived backscatter images (Long and Drinkwater, 1994). The NASA Scatterometer (NSCAT) operated on the Advanced Environmental Observation Satellite (ADEOS) from September 1996 to June 1997 and also permitted study of melt zones on Greenland (Long and Drinkwater, 1999). Timing of melt onset was detected by Nghiem *et al.* (2001) on the Greenland Ice Sheet by a sharp decrease in backscatter, and verified with *in situ* measurements, using the SeaWinds scatterometer on the QuikSCAT satellite.

For seasonal snow cover, Nghiem and Tsai (2001) show that NSCAT backscatter patterns reveal boundaries that correspond to various snow classes as defined by Sturm *et al.* (1995). Additionally, they show rapid changes in the backscatter over the northern plains of the United States and the Canadian prairies that led to the major spring 1997 floods in the mid-western United States and southern Canada (Figure 7).

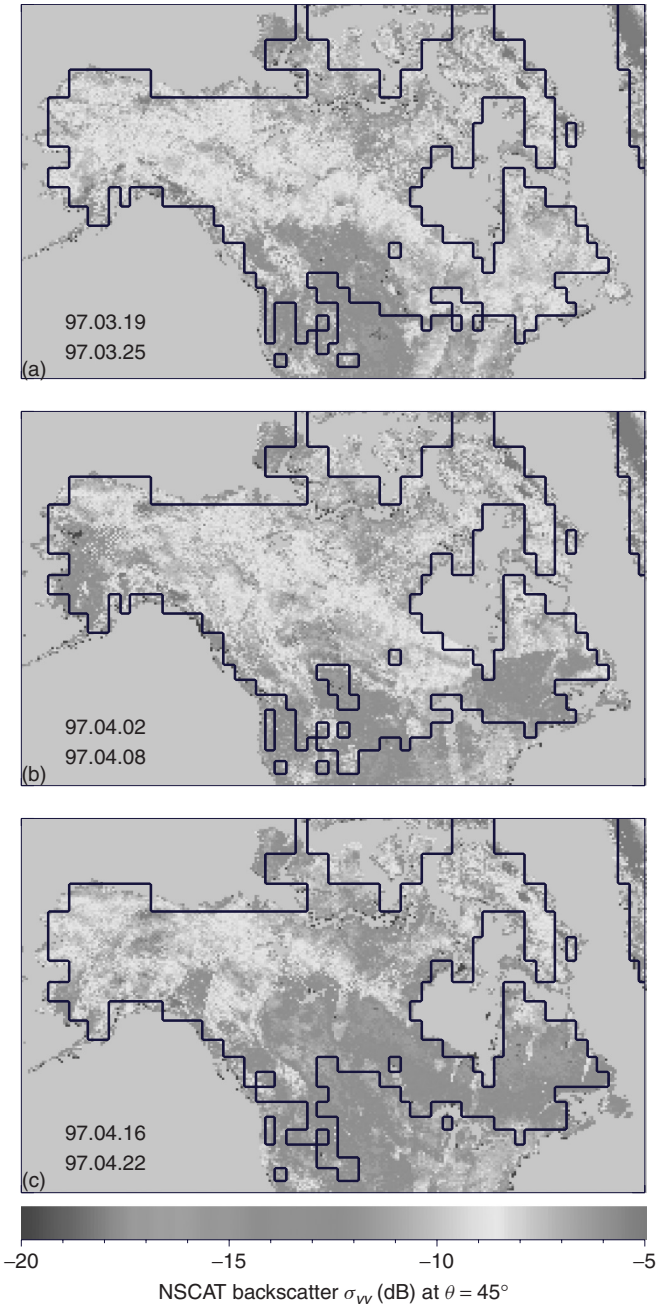

Figure 7 NSCAT backscatter signatures over snow cover corresponding to snow events leading to the 1997 flood in the northern plains of the United States and the Canadian prairies: (a) period of snowmelt from March 19 to March 25, 1997; (b) period of the blizzard from April 2 to April 8, 1997; and (c) period of rapid snow retreat from April 16 to April 22, 1997 (Nghiem *et al.*, 2001). (©2001 IEEE, Courtesy of Son Nghiem, Jet Propulsion Laboratory, Pasadena, CA). A color version of this image is available at http://www.mrw.interscience.wiley.com/ehs

Future Directions and Conclusions

Mapping snow cover areal extent using satellite observations is relatively mature and well validated (see, e.g., Robinson, 1993, 1999; Hughes *et al.*, 1996; Frei *et al.*, 1999; Hall *et al.*, 2002a; Brown *et al.*, 2003; Mauer *et al.*, 2003). Recent global water and climate system studies have begun to examine the link between snow cover areal extent and atmospheric dynamics. For example, Cohen and Entekhabi (1999) investigated the link between early season snow extent in Eurasia and the dynamics of the Siberian high. Saunders *et al.* (2003) show a link between summer snow extent and the winter North Atlantic Oscillation. These studies are important for our understanding of the role of snow in the Earth's hydrological cycle and how it affects human sustainability, especially in regions that are heavily dependent on snowmelt runoff for water supply.

The methodology to map global SWE from remote-sensing instruments is less mature. While microwave remote-sensing observations are helping to advance our ability to effectively characterize water storage in snowpacks, there remain uncertainties about the retrievals from these instruments. Historically, the frequency configurations of space borne active radar systems have produced measurements that are sensitive to the presence or absence of wet snow only and little or no direct information about SWE can be determined from these instruments. Satellite passive microwave measurements now have a 25- year record from which SWE can be estimated. However, with the characteristically large instantaneous fields of view that characterize these instruments (tens of kilometers), the uncertainties associated with SWE estimates are difficult to quantify, and, therefore, are still under investigation. Studies have shown that in noncomplex terrain with low-stand vegetation, reasonable estimates of SWE can be obtained from passive microwave measurements. In other terrain types, however, larger uncertainties persist.

In order to characterize snow water storage, new and improved satellite instrument measurement techniques need to be developed, especially for instruments in the microwave part of the electromagnetic spectrum that are sensitive to snow volume. Ku-band radar measurements are sensitive to SWE and could be developed to resolve fine spatial variations of SWE (tens of meters) through SAR technology. For passive microwave measurements, the relatively low spatial resolution is a key cause of uncertainties in the estimation of SWE. Only through technology improvements in antenna design can instantaneous fields of view be significantly improved, thus increasing the spatial resolution (e.g. Doiron *et al.*, 2004).

With improvements in microwave instrument and measurement techniques of SWE, the uncertainties and errors in SWE estimates will be reduced providing more confidence in our ability to estimate snow water storage throughout the year. If these technology developments come to fruition and new, "more SWE-capable" microwave missions overlap with the current and planned global multidisciplinary instruments, such as the available AMSR-E and the proposed Conical Scanning Microwave Imager/Sounder (CMIS) planned for National Polar-orbiting Operational Environmental Satellite System (NPOESS), the benefits could be great (Kelly *et al.*, 2004). Local scale SWE characterization would be possible; the prospect of combining high spatial resolution-accurate SWE measurements with sophisticated numerical land surface models may then be possible, and is a very exciting one from the water resource management perspective.

Satellite remote sensing has been used to map snow cover for nearly 40 years. Decade-scale CDR-quality records of snow-covered area are already in existence for the Northern Hemisphere (Robinson and Frei, 2000) and are useful in climate models, however, problems exist in developing a CDR for SWE (Armstrong and Brodzik, 2001; Derksen *et al.*, 2003), as discussed above. We can now extend the snow-covered area record using SMMR, SSM/I MODIS, and AMSR data to the global scale, and provide CDR-quality maps of snow-covered area, and continue to study the development of CDR-quality datasets of SWE and snow albedo using visible, near infrared, and passive microwave sensors such as the MODIS and AMSR.

The trend has been toward increasingly automatically processed quantitative maps with error bars provided. Automated processing is necessary so that consistent products can be derived from the observations and long duration data sets might ultimately be available for long-term water-cycle studies. The error estimates associated with snow products are also essential if the products are to be used effectively in combination with catchment-based land surface or climate models. This is because models that require snow-state parameters often require the errors associated with the estimated snow states, especially if data assimilation techniques are used to generate blended products. Whether the snow products are used for initial conditioning or as a forcing variable in a model, or whether the products are used in their own right, the role of remotely sensed observations of snow will continue to be important and is set to play an increasingly important role in climate and hydrological forecasting.

Future sensors will permit automated algorithms to be used to create maps that are consistent with existing maps so that the confidence level of the long-term (~40 year) record is high. The quality allows them to be amenable to comparison with long-term records of other geophysical parameters such as global sea ice, and for input to general circulation models.

Acknowledgments

The authors would like to thank Dr. Andrew G. Klein of Texas A & M University for helpful comments on parts of the manuscript.

REFERENCES

Anderson T. (1982) Operational snow mapping by satellites. *Hydrological Aspects of Alpine and High Mountain Areas, Proceedings of the Exeter Symposium*, July 1982, IAHS Publication 138: pp. 149–154.

Armstrong R.L. and Brodzik M.J. (1998) A comparison of northern hemisphere snow extent derived from passive microwave and visible remote-sensing data. *Proceedings of IGARSS'98, 18th International Geoscience and Remote Sensing Symposium*, 6–10 July 1998, Vol. 3, IEEE: Seattle, pp. 1255–1257.

Armstrong R.L. and Brodzik M.J. (2001) Recent northern hemisphere snow extent: a comparison of data derived from visible and microwave satellite sensors. *Geophysical Research Letters*, **28**(19), 3673–3676.

Armstrong R.L. and Brodzik M.J. (2002) Hemispheric-scale comparison and evaluation of passive-microwave snow algorithms. *Annals of Glaciology*, **34**, 38–44.

Bader, H. (1962) *The Physics and Mechanics of Snow as a Material*, Cold Regions Research and Engineering Laboratory: Hanover, Report II-B, p. 1.

Barry R. (1983) Research on snow and ice. *Reviews of Geophysics and Space Physics*, **21**, 765–776.

Barry R. (1984) Possible CO_2-induced warming effects on the cryosphere. *Climatic Changes on a Yearly to Millennial Basis*, D. Reidel Publishing Company: pp. 571–604.

Barry R. (1990) Evidence of recent changes in global snow and ice cover. *GeoJournal*, **20**(2), 121–127.

Basist A., Garrett D., Ferraro R., Grody N. and Mitchell K. (1996) A comparison between snow cover products derived from visible and microwave satellite observations. *Journal of Applied Meteorology*, **35**(2), 163–177.

Bauer K.G. and Dutton J.A. (1962) Albedo variations measured from an airplane over several types of surface. *Journal of Geophysical Research*, **67**(6), 2367–2376.

Bernier P.Y. (1987) Microwave remote sensing of snowpack properties: potential and limitations. *Nordic Hydrology*, **18**, 1–20.

Bernier M. and Fortin J.-P. (1998) The potential of time series of C-band SAR data to monitor dry and shallow snow cover.

IEEE Transactions on Geoscience and Remote Sensing, **36**(1), 226–243.

Bernier M., Fortin J.-P., Gauthier Y., Gauthier R., Roy R. and Vincent P. (1999) Determination of snow water equivalent using RADARSAT SAR in eastern Canada. *Hydrological Processes*, **13**, 3041–3051.

Brest C.L. and Goward S.N. (1987) Deriving surface albedo measurements from narrow band satellite data. *International Journal of Remote Sensing*, **8**(3), 351–367.

Brown R.D. (2000) Northern hemisphere snow cover variability and change, 1915–1997. *Journal of Climate*, **13**, 2339–2355.

Brown R.D., Brasnett B. and Robinson D. (2003) Gridded North American monthly snow depth and snow water equivalent for GCM evaluation. *Atmosphere-Ocean*, **41**(1), 1–14.

Brown R.D. and Goodison B.E. (1996) Interannual variability in reconstructed Canadian snow cover, 1915–1992. *Journal of Climate*, **9**, 1299–1318.

Bunting J.T. and d'Entremont R.P. (1982) *Improved Cloud Detection Utilizing Defense Meteorological Satellite Program Near Infrared Measurements*, Air Force Geophysics laboratory: Hanscom AFB, AFGL-TR-82-0027, Environmental Research Papers No. 765, p. 91.

Bussières N., De Sève D. and Walker A. (2002) Evaluation of MODIS snow-cover products over Canadian regions. *Proceedings of IGARSS'02*, dates, Toronto, pp. 2302–2304.

Carroll T.R. (1987) Operational airborne measurements of snow water equivalent and soil moisture using terrestrial gamma radiation in the United States. *Large Scale Effects of Seasonal Snow Cover Proceedings of the Vancouver Symposium*, August 1987, IAHS Publication No. 166: pp. 213–223.

Carroll T.R. (1995) Remote sensing of snow in the cold regions. *Proceedings of the First Moderate Resolution Imaging Spectroradiometer (MODIS) Snow and Ice Workshop*, 13–14 September, 1995, NASA Conference Publication 3318: Greenbelt, pp. 3–14.

Carroll T., Cline D., Fall G., Nilsson A., Li L. and Rost A. (2001) NOHRSC operations and the simulation of snow cover properties for the coterminous U.S. *Proceedings of the 69th Western Snow Conference*, Sun Valley, 16–19 April 2001.

Chang A.T.C., Foster J.L. and Hall D.K. (1987) Nimbus-7 SMMR derived global snow cover parameters. *Annals of Glaciology*, **9**, 39–44.

Chang A.T.C., Foster J.L., Hall D.K., Rango A. and Hartline B.K. (1982) Snow water equivalent estimation by microwave radiometry. *Cold Regions Science and Technology*, **5**(3), 259–267.

Chang A.T.C., Gloersen P., Schmugge T.J., Wilheit T. and Zwally H.J. (1976) Microwave emission from snow and glacier ice. *Journal of Glaciology*, **16**(74), 23–39.

Chang A.T.C., Kelly R.E.J., Foster J.L. and Hall D.K. (2003) Estimation of global snow cover using passive microwave data. *Proceedings of the International Society for Optical Engineering (SPIE)*, Hangshou, pp. 381–390, 24–25 October 2002.

Choudhury B.J. and Chang A.T.C. (1979) Two-stream theory of reflectance of snow. *IEEE Transactions on Geoscience and Remote Sensing*, **GE-17**(3), 63–68.

Cline D.W., Bales R.C. and Dozier J. (1998) Estimating the spatial distribution of snow in mountain basins using remote sensing and energy balance modeling. *Water Resources Research*, **34**(5), 1275–1285.

Cohen J. and Entekhabi D. (1999) Eurasian snow cover variability and northern hemisphere climate predictability. *Geophysical Research Letters*, **26**, 345–348.

Colbeck S.C. (1982) An overview of seasonal snow metamorphism, *Reviews of Geophysics and Space Physics*, **20**(1), 45–61.

Crane R.G. and Anderson M.R. (1984) Satellite discrimination of snow/cloud surfaces. *International Journal of Remote Sensing*, **5**(1), 213–223.

Derksen C., Walker A., LeDrew E. and Goodison B. (2002) Time series analysis of passive-microwave-derived central North American snow water equivalent imagery. *Annals of Glaciology*, **34**, 1–7.

Derksen C., Walker A., LeDrew E. and Goodison B. (2003) Combining SMMR and SSM/I data for time series analysis of central North American snow water equivalent. *Journal of Hydrometeorology*, **4**, 304–316.

Dewey K.F. and Heim R. Jr (1981) *Satellite Observations of Variation in Northern Hemisphere Seasonal Snow Cover*, NOAA Technical Report NESS 87: Washington, DC, p. 83.

Dewey K.F. and Heim R. Jr (1983) *Satellite Observations of Variations in Southern Hemisphere Snow Cover*, NOAA Technical Report NESDIS 1: p. 20.

Dirmhirn I. and Eaton F. (1975) Some characteristics of the albedo of snow. *Journal of Applied Meteorology*, **14**, 375–379.

Doiron T.A., Piepmeier J.R., Hilliard L.M., Shirgur B., Kelly R.E.J., Kim E.J. and Cline D. (2004) One dimensional synthetic aperture radiometer using a parabolic cylinder reflector. *Proceedings of 2004 IEEE Aerospace Conference*, 6–13 March, Montana.

Dozier J. (1984) Snow reflectance from Landsat-4 thematic mapper. *IEEE Transactions on Geoscience and Remote Sensing*, **GE-22**(3), 323–328.

Dozier J. (1987) Recent research in snow hydrology. *Reviews of Geophysics*, **25**(2), 153–161.

Dozier J. (1989) Spectral signature of alpine snow cover from the Landsat thematic mapper. *Remote Sensing of Environment*, **28**, 9–22.

Dozier J. and Painter T.H. (2004) Multispectral and hyperspectral remote sensing of alpine snow properties. *Annual Reviews of Earth and Planetary Science*, **32**, 465–494.

Dozier J., Schneider S.R. and McGinnis D.F. Jr (1981) Effect of grain size and snowpack water equivalence on visible and near-infrared satellite observations of snow. *Water Resources Research*, **17**, 1213–1221.

Duguay C. and LeDrew E.F. (1992) Estimating surface reflectance and albedo from Landsat-5 thematic mapper over rugged terrain. *Photogrammetric Engineering and Remote Sensing*, **58**(5), 551–558.

Evans S. (1965) The dielectric properties of ice and snow – a review. *Journal of Glaciology*, **5**, 773–792.

Foster J.L., Barton J.S., Chang A.T.C. and Hall D.K. (2000) Snow crystal orientation effects on the scattering of passive microwave radiation. *IEEE Transactions on Geoscience and Remote Sensing*, **38**(5), 2430–2433.

Foster J.L., Chang A.T.C. and Hall D.K. (1997) Comparison of snow mass estimates from a prototype passive microwave snow

algorithm, a revised algorithm and snow depth climatology. *Remote Sensing of Environment*, **62**, 132–142.

Foster J.L., Chang A.T.C., Hall D.K., Wergin W.P., Erbe E.F. and Barton J. (1999) Effect of snow crystal shape on the scattering of passive microwave radiation. *IEEE Transactions on Geoscience and Remote Sensing*, **37**(2), 1165–1168.

Foster J.L., Hall D.K. and Chang A.T.C. (1987) Remote sensing of snow. *EOS Transactions, American Geophysical Union*, **68**(32), 681–684.

Foster J., Liston G., Koster R., Essery R., Behr H., Dumenil L., Verseghy D., Thompson S., Pollard D. and Cohen J. (1996) Snow cover and snow mass intercomparisons of general circulation models and remotely sensed datasets. *Journal of Climate*, **9**(2), 409–426.

Foster J.L., Sun C., Walker J.P., Kelly R., Chang A., Dong J. and Powell H. (2005) Quantifying the uncertainty in passive microwave snow water equivalent observations, *Remote Sensing of Environment*, **94**, 187–203.

Frei A. and Robinson D.A. (1999) Northern hemisphere snow extent: regional variability 1972–1994. *International Journal of Climatology*, **19**, 1535–1560.

Frei A., Robinson D.A. and Hughes M.G. (1999) North American snow extent: 1900–1994. *International Journal of Climatology*, **19**, 1517–1534.

Gauthier Y., Bernier M., Fortin J.-P., Gauthier R., Roy R. and Vincent P. (2001) Operational determination of snow water equivalent using Radarsat data over a large hydroelectric complex in eastern Canada. *Proceedings of a Symposium on Remote Sensing and Hydrology 2000*, Santa Fe, April 2000, Owe M., Brubaker K., Ritchie J. and Rango A. (Eds.), IAHS Publication No. 267: 343–348.

Gerland S., Winther J.-G., Orbaek J.B., Liston G.E., Oritsland N.A., Blanco A. and Ivanov B. (1999) Physical and optical properties of snow covering Arctic tundra on Svalbard. *Hydrological Processes*, **13**, 2331–2343.

Goita K., Walker A.E. and Goodison B.E. (2003) Algorithm development for the estimation of snow water equivalent in the boreal forest using passive microwave data. *International Journal of Remote Sensing*, **24**(5), 1097–1102.

Goodison B. (1989) Determination of areal snow water equivalent on the Canadian Prairies using passive microwave satellite data. *Proceedings of the IGARSS'89 Symposium*, Vancouver, pp. 1243–1246, July 1989.

Goodison B.E., Rubinstein I., Thirkettle F.W. and Langham E.J. (1986) Determination of snow water equivalent on the Canadian prairies using microwave radiometry. *Modelling Snowmelt-Induced Processes, Proceedings of the Budapest Symposium*, July 1986, IAHS Publication No. 155: pp. 163–173.

Goodison B. and Walker A. (1994) Canadian development and use of snow cover information from passive microwave satellite data. In *Proceedings of the ESA/NASA International Workshop*, Choudhury B.J., Kerr Y.H., Njoku E.G. and Pampaloni P. (Eds.), pp. 245–262.

Goodison B.E., Waterman S.E. and Langham E.J. (1980) Application of synthetic aperture radar data to snow cover monitoring. *Proceedings of the 6th Canadian Symposium on Remote Sensing*, Halifax, pp. 263–271, 21–23 May 1980.

Grenfell T.C. and Maykut G.A. (1977) The optical properties of snow and ice in the arctic basin. *Journal of Glaciology*, **18**, 445–463.

Grenfell T.C., Perovich D.K. and Ogren J.A. (1981) Spectral albedos of an alpine snowpack. *Cold Regions Science and Technology*, **4**, 121–127.

Greuell W. and de Ruyter de Wildt M. (1999) Anisotropic reflectance by melting glacier ice: measurements and parameterizations in Landsat TM bands 2 and 4. *Remote Sensing of Environment*, **70**, 265–277.

Greuell W., Reijmer C.H. and Oerlemans J. (2002) Narrowband-to-broadband albedo conversion for glacier ice and snow based on aircraft and near-surface measurements. *Remote Sensing of Environment*, **82**, 48–63.

Grody N. and Basist A. (1996) Global identification of snowcover using SSM/I measurements. *IEEE Transactions on Geoscience and Remote Sensing*, **34**(1), 237–249.

Guneriussen T., Hogda K.A., Johnsen H. and Lauknes I. (2001) InSAR for estimation of changes in snow water equivalent of dry snow. *IEEE Transactions on Geoscience and Remote Sensing*, **39**(10), 2101–2108.

Hall D.K., Chang A.T.C. and Foster J.L. (1986) Detection of the depth-hoar layer in the snow-pack of the Arctic coastal plain of Alaska, U.S.A., using satellite data. *Journal of Glaciology*, **32**(110), 87–94.

Hall D.K., Chang A.T.C., Foster J.L., Benson C.S. and Kovalick W.M. (1989) Comparison of in situ and satellite-derived reflectances of glacier. *Remote Sensing of Environment*, **28**, 23–31.

Hall D.K., Foster J.L. and Chang A.T.C. (1982) Measurement and modeling of microwave emission from forested snowfields in Michigan. *Nordic Hydrology*, **13**, 129–138.

Hall D.K., Foster J.L., Salomonson V.V., Klein A.G. and Chien J.Y.L. (2001) Development of a technique to assess snow-cover mapping errors from space. *IEEE Transactions on Geoscience and Remote Sensing*, **39**(2), 432–438.

Hall D.K., Riggs G.A., Salomonson V.V., DiGirolamo N.E. and Bayr K.J. (2002a) MODIS snow-cover products. *Remote Sensing of Environment*, **83**, 181–194.

Hall D.K., Kelly R.J.E., Riggs G.A., Chang A.T.C. and Foster J.L. (2002b) Assessment of the relative accuracy of hemispheric-scale snow-cover maps. *Annals of Glaciology*, **34**, 24–30.

Hallikainen M. (1984) Retrieval of snow water equivalent from Nimbus-7 SMMR data: effect of land-cover categories and weather conditions. *IEEE Journal of Oceanic Engineering*, **OE-9**(5), 372–376.

Hallikainen M.T. and Jolma P.A. (1992) Comparison of algorithms for retrieval of snow water equivalent from Nimbus-7 SMMR data in Finland. *IEEE Transactions on Geoscience and Remote Sensing*, **30**(1), 124–131.

Hallikainen M. and Ulaby F.T. (1986) Dielectric and scattering behaviour of snow at microwave frequencies. *Proceedings of the International Geoscience and Remote Sensing Symposium*, Zurich, pp. 87–91, 8–11 September 1986.

Hansen J. and Nazarenko L. (2004) Soot climate forcing via snow and ice albedos. *Proceedings of the National Academy of Sciences*, **101**(2), 423–428.

Hanson K.J. and Viebrock H.J. (1964) Albedo measurements over the northeastern United States. *Monthly Weather Review*, **92**(5), 223–234.

Hobbs P.V. (1974) *Ice Physics*, Clarendon Press: Oxford, p. 837.

Hughes M.G., Frei A. and Robinson D.A. (1996) Historical analysis of North American snow cover extent: merging satellite and station derived snow cover observations. *Proceedings of the 1996 Eastern Snow Conference*, Williamsburg, pp. 21–32.

Hughes M.G. and Robinson D.A. (1996) Historical snow cover variability in the great plains region of the USA: 1910 through to 1993. *International Journal of Climatology*, **16**, 1005–1018.

Josberger E., Campbell W.J., Gloersen P., Chang A.T.C. and Rango A. (1993) Snow conditions and hydrology of the upper Colorado River Basin from satellite passive microwave observations. *Annals of Glaciology*, **17**, 322–326.

Kaufman Y.J., Kleidman R.G., Hall D.K., Martins V.J. and Barton J.S. (2002) Remote sensing of subpixel snow cover using 0.66 and 2.1 μm channels. *Geophysical Research Letters*, **29**(16), doi: 10.1029/2001GL013580.

Kelly R.E.J. (2001) Remote sensing of UK snow covers using multi-sensor satellite imagery. *Proceedings of a Symposium on Remote Sensing and Hydrology 2000*, April 2000, IAHS Publication No. 267: Santa Fe, pp. 72–75.

Kelly R.E.J. and Chang A.T.C. (2003) Development of a passive microwave global snow depth retrieval algorithm for SSM/I and AMSR-E data. *Radio Science*, **38**(4), doi: 10.1029/2002RS002648.

Kelly R.E.J., Chang A.T.C., Foster J.L. and Hall D.K. (2004) Using remote sensing and spatial models to monitor snow depth and snow water equivalent. In *Spatial Modelling of the Terrestrial Environment*, Kelly R.E.J., Drake N.A. and Barr S.L. (Eds.), John Wiley & Sons: pp. 35–58.

Kelly R.E.J., Chang A.T.C., Tsang L. and Foster J.L. (2003) A prototype AMSR-E global snow area and snow depth algorithm. *IEEE Transactions Geoscience and Remote Sensing*, **41**(2), 230–242.

Klein A.G., Hall D.K. and Riggs G.A. (1998) Improving snow-cover mapping in forests through the use of a canopy reflectance model. *Hydrological Processes*, **12**, 1723–1744.

Klein A.G. and Stroeve J. (2002) Development and validation of a snow albedo algorithm for the MODIS instrument. *Annals of Glaciology*, **34**, 45–52.

Knap W.H. and Oerlemans J. (1996) The surface albedo of the Greenland ice sheet: satellite-derived and in situ measurements in the Søndre Strømfjord area during the 1991 melt season. *Journal of Glaciology*, **42**(141), 364–374.

Knap W.H. and Reijmer C.H. (1998) Anisotropy of the reflected radiation field over melting glacier ice: measurements in Landsat TM bands 2 and 4. *Remote Sensing of Environment*, **65**, 93–104.

Knap W.H., Reijmer C.H. and Oerlemans J. (1998) Narrowband to broadband conversion of Landsat TM glacier albedos. *International Journal of Remote Sensing*, **20**(10), 2091–2110.

König M., Winther J.-G. and Isaksson E. (2001) Measuring snow and glacier ice properties from satellite. *Reviews of Geophysics*, **39**(1), 1–27.

Koskinen J.T., Pulliainen J.T. and Hallikainen M.T. (1997) The use of ERS-1 SAR data in snow melt monitoring. *IEEE Transactions on Geoscience and Remote Sensing*, **35**, 601–610.

Kukla G. and Robinson D.A. (1980) Annual cycle of surface albedo. *Monthly Weather Review*, **108**, 56–68.

Kunzi K.F., Fisher A.D. and Staelin D.H. (1976) Snow and ice surfaces measured by the Nimbus-5 microwave spectrometer. *Journal of Geophysical Research*, **81**, 4965–4980.

Kunzi K.F., Patil S. and Rott H. (1982) Snow-cover parameters retrieved from Nimbus-7 Scanning Multichannel Microwave Radiometer (SMMR) data. *IEEE Transactions on Geoscience and Remote Sensing*, **GE-20**(4), 452–467.

Kurvonen L. and Hallikainen M. (1997) Influence of land-cover category on brightness temperature of snow. *IEEE Transactions on Geoscience and Remote Sensing*, **35**(2), 367–377.

Kyle H.L., Curran R.J., Barnes W.L. and Escoe D. (1978) A cloud physics radiometer. *Third Conference on Atmospheric Radiation*, Davis, pp. 108–109.

Leconte R. (1995) Exploring the behaviour of microwaves in a snowpack using modelling techniques. *Canadian Journal of Remote Sensing*, **22**(1), 23–35.

Leconte R., Carroll T. and Tang P. (1990) Preliminary investigations on monitoring the snow water equivalent using synthetic aperture radar. *Proceedings of the Eastern Snow Conference*, Bangor, pp. 73–86, 7–8 June, 1990.

Ledley T.S., Sundquist E.T., Schwartz S.E., Hall D.K., Fellows J.D. and Killeen T.L. (1999) Climate change and greenhouse gases. *EOS Transactions, American Geophysical Union*, **80**(39), 453–454, 457–458.

Liang S. (2000) Narrow to broadband conversion of land surface albedo I: algorithms. *Remote Sensing of Environment*, **76**, 213–238.

Long D.G. and Drinkwater M.R. (1994) Greenland ice-sheet surface properties observed by the Seasat-A scatterometer at enhanced resolution. *Journal of Glaciology*, **40**(135), 213–230.

Long D.G. and Drinkwater M.R. (1999) Cryosphere applications of NSCAT data. *IEEE Transactions on Geoscience and Remote Sensing*, **37**(3), 1671–1684.

Long M.W. (1975) *Radar Reflectivity of Land and Sea*, D.C. Heath & Company: Lexington.

Male D.H. (1980) The seasonal snowcover. In *Dynamics of Snow and Ice Masses*, Colbeck S. (Ed.), Academic Press: New York, pp. 305–395.

Martinelli M. Jr (1979) Research on snow and ice. *Reviews of Geophysics and Space Physics*, **17**(6), 1253–1288.

Matson M., Roeplewski C.F. and Varnadore M.S. (1986) *An Atlas of Satellite-Derived Northern Hemisphere Snow Cover Frequency*, National Weather Service: Washington, p. 75.

Mätzler C. (1987) Applications on the interactions of microwaves with the natural snow cover. *Remote Sensing Reviews*, **2**, 259–387.

Mätzler C. (1997) Autocorrelation functions of granular media with arrangement of spheres, spherical shells or ellipsoids. *Journal of Applied Physics*, **3**, 1509–1517.

Mätzler C. and Schanda E. (1984) Snow mapping with active microwave sensors. *International Journal of Remote Sensing*, **5**(2), 409–422.

Mauer E.P., Rhoads J.D., Dubayah R.O. and Lettenmaier D.P. (2003) Evaluation of the snow-covered area data product from MODIS. *Hydrological Processes*, **17**, 59–71.

McFadden J.D. and Ragotzkie R.A. (1967) Climatological significance of albedo in central Canada. *Journal of Geophysical Research*, **72**(4), 1135–1143.

Meier M. (1972) Measurement of snow cover using passive microwave radiation. *International Symposia on the Role of Snow and Ice in Hydrology, Proceedings of the Banff Symposium*, Banff, pp. 739–750, September, 1972.

Mekler Y. and Joseph J.H. (1983) Direct determination of surface albedos from satellite imagery. *Journal of Climate and Applied Meteorology*, **22**, 530–558.

Mognard N.M. and Josberger E.G. (2002) Northern Great Plains 1996/97 seasonal evolution of snowpack parameters from satellite passive-microwave measurements. *Annals of Glaciology*, **34**, 15–23.

Nagler T. and Rott H. (2000) Retrieval of wet snow by means of multitemporal SAR data. *IEEE Transactions on Geoscience and Remote Sensing*, **38**(2), 754–765.

Nghiem S.V., Steffen K., Kwok R. and Tsai W.Y. (2001) Detection of snowmelt regions on the Greenland ice sheet using diurnal backscatter change. *Journal of Glaciology*, **47**(159), 539–547.

Nghiem S.V. and Tsai W-Y (2001) Global snow cover monitoring with space borne Ku-band scatterometer. *IEEE Transactions on Geoscience and Remote Sensing*, **39**(10), 2118–2134.

Nicodemus F.E., Hsia F.C., Richmond J.J., Ginsberg I.W. and Limperis T. (1977) Geometrical considerations and nomenclature for reflectance, *Technical Report Monograph, 160*, National Bureau of Standards: Gaithersburg.

Nolin A.W., Dozier J. and Mertes L.A.K. (1993) Mapping alpine snow using a spectral mixture modeling technique. *Annals of Glaciology*, **17**, 121–124.

Nolin A.W. and Liang S. (2000) Progress in bidirectional reflectance modeling and applications for surface particulate media: snow and soils. *Remote Sensing Reviews*, **18**, 307–342.

Nolin A.W. and Stroeve J.C. (1997) The changing albedo of the Greenland ice sheet: implications for climate change. *Annals of Glaciology*, **25**, 51–57.

O'Brien H.W. and Munis R.H. (1975) Red and near-infrared spectral reflectance of snow, *Operational Applications of Satellite Snowcover Observations*, a workshop held in South Lake Tahoe, 18–20 August, 1975, NASA SP-391.

Painter T.H., Dozier J., Roberts D.A., Davis R.E. and Green R.O. (2003) Retrieval of subpixel snow-covered area and grain size from imaging spectrometer data. *Remote Sensing of Environment*, **85**, 64–77.

Pivot F.C., Kergomard C. and Duguay C.R. (2002) Use of passive-microwave data to monitor spatial and temporal variations of snow cover at tree line, near Churchill, Manitoba, Canada. *Annals of Glaciology*, **34**, 58–64.

Pomeroy J.W. and Gray D.M. (1995) *Snowcover Accumulation, Relocation and Management*, National Hydrology Research Institute: Environment Canada, NHRI Science Report No. 7, p. 134.

Potts H.L. (1937) A photographic snow survey method of forecasting from photographs. *Transactions of the American Geophysical Union*, South Continental Divide Snow Survey Conference: pp. 658–660.

Ramage J.M. and Isacks B.L. (2002) Determination of melt-onset and refreeze timing on southeast Alaskan icefields using SSM/I diurnal amplitude variations. *Annals of Glaciology*, **34**, 391–398.

Ramsay B. (1998) The interactive multisensor snow and ice mapping system. *Hydrological Processes*, **12**, 1537–1546.

Rango A. and Martinec J. (1979) Application of a snowmelt-runoff model using Landsat data. *Nordic Hydrology*, **10**, 225–238.

Rango A. and Martinec J. (1982) Snow accumulation derived from modified depletion curves of snow coverage. *Symposium on Hydrological Aspects of Alpine and High Mountain Areas*, in Exeter, IAHS Publication No. 138: pp. 83–90.

Rango A. and Salomonson V.V. (1977) Seasonal streamflow estimation in the Himalayan region employing meteorological satellite snow cover observations. *Water Resources Research*, **13**(1), 109–112.

Rango A., Wergin W.P. and Erbe E.F. (1996) Snow crystal imagery uses SEM, Part II metamorphosed snow. *Hydrological Sciences Journal*, **41**, 235–250.

Riggs G.A. and Hall D.K. (2004) Snow mapping with the MODIS Aqua instrument. *Proceedings of the 61st Eastern Snow Conference*, Portland, 9–11 June 2004, pp. 81–84.

Robinson D.A. (1993) Hemispheric snow cover from satellites. *Annals of Glaciology*, **17**, 367–371.

Robinson D.A. (1997) Hemispheric snow cover and surface albedo for model validation. *Annals of Glaciology*, **25**, 241–245.

Robinson D.A. (1999) Northern hemisphere snow cover during the satellite era. *Proceedings of the 5th Conference Polar Meteorology and Oceanography*, American Meteorological Society: Boston, Dallas, pp. 255–260.

Robinson D.A., Dewey K.F. and Heim R.R. (1993) Global snow-cover monitoring: an update. *Bulletin of the American Meteorological Society*, **74**(9), 1689–1696.

Robinson D.A. and Frei A. (2000) Seasonal variability of northern hemisphere snow extent using visible satellite data. *Professional Geographer*, **51**, 307–314.

Robinson D.A. and Kukla G. (1985) Maximum surface albedo of seasonally snow-covered lands in the northern hemisphere. *Journal of Climate and Applied Meteorology*, **24**, 402–411.

Robinson D.A., Scharfen G., Serreze M.C., Kukla G. and Barry R.G. (1986) Snow melt and surface albedo in the arctic basin. *Geophysical Research Letters*, **13**, 945–948.

Robinson D.A., Serreze M.C., Barry R.G., Scharfen G. and Kukla G. (1992) Large-scale patterns and variability of snowmelt and parameterized surface albedo in the arctic basin. *Journal of Climate*, **5**(10), 1109–1119.

Robock A. (1980) The seasonal cycle of snow cover, sea ice and surface albedo. *Monthly Weather Review*, **108**, 267–285.

Romanov P., Gutman G. and Csiszar I. (2000) Automated monitoring of snow cover over North America with multispectral satellite data. *Journal of Applied Meteorology*, **39**, 1866–1880.

Romanov P. and Tarpley D. (2003) Automated monitoring of snow cover over South America using GOES imager

data. *International Journal of Remote Sensing*, **24**(5), 1119–1125.

Rosenthal W. and Dozier J. (1996) Automated mapping of montane snow cover at subpixel resolution from the Landsat thematic mapper. *Water Resources Research*, **32**(1), 115–130.

Ross B. and Walsh J.E. (1987) A comparison of simulated and observed fluctuations in summertime arctic surface albedo. *Journal of Geophysical Research*, **92**(C12), 13115–13125.

Rott H. (1984) The analysis of backscattering properties from SAR data of mountainous regions. *IEEE Journal of Oceanic Engineering*, **OE-0**, 347–355.

Rott H., Davis R.E. and Dozier J. (1992) Polarimetric and multifrequency SAR signatures of wet snow. *Proceedings of the International Geoscience and Remote Sensing Symposium 1992*, Houston, pp. 1658–1660, 26–29 May, 1992.

Rott H., Künzi K. and Patil S. (1981) Temporal and spatial variations of snow properties derived from Nimbus-7 SMMR data. 20th URSI General Assembly, Symposium of Remote Sensing, Washington, August 10–19, 1981.

Rott H. and Mätzler C. (1987) Possibilities and limits of synthetic aperture radar for snow and glacier surveying. *Annals of Glaciology*, **9**, 195–199.

Rott H. and Nagler T. (1993) Capabilities of ERS-1 SAR for snow and glacier monitoring in alpine areas. *Proceedings of the Second ERS-1 Symposium*, 1–6, ESA SP-359.

Rott H. and Nagler T. (1995) Monitoring temporal dynamics of snowmelt with ERS-1 SAR. *Proceedings of IGARSS 95*, Fierenze, pp. 1747–1749, 10–14 July.

Salomonson V.V. and Appel I.L. (2004) Estimating the fractional snow covering using the normalized difference snow index. *Remote Sensing of Environment*, **89**, 351–360.

Salomonson V.V. and Marlatt W.E. (1968) Anisotropic solar reflectance over white sand, snow and stratus clouds. *Journal of Applied Meteorology*, **7**(3), 475–483.

Saunders M.A., Qian B. and Lloyd-Hughes B. (2003) Summer snow extent heralding of the winter North Atlantic Oscillation. *Geophysical Research Letters*, **30**(7), 1378, doi:10.1029/2002GL016832.

Schanda E., Mätzler C. and Künzi K. (1983) Microwave remote sensing of snow cover. *International Journal of Remote Sensing*, **4**(1), 149–158.

Scharfen G., Barry R.G., Robinson D.A., Kukla G. and Serreze M.C. (1987) Large-scale patterns of snow melt on Arctic sea ice mapped from meteorological satellite imagery. *Annals of Glaciology*, **9**, 1–6.

Scharfen G.R., Hall D.K., Khalsa S.J.S., Wolfe J.D., Marquis M.C., Riggs G.A. and McLean B. (2000) Accessing the MODIS snow and ice products at the NSIDC DAAC. *Proceedings of IGARSS'00*, Honolulu, pp. 2059–2061, 23–28 July 2000.

Serreze M.C., Walsh J.E., Chapin F.S. III, Osterkamp T., Dyurgerov M., Romanovsky V., Oechel W.C., Morison J., Zhang T. and Barry R.G. (2000) Observational evidence of recent change in the northern high-latitude environment. *Climate Change*, **46**, 159–207.

Shi J. and Dozier J. (1997) Mapping seasonal snow with SIR-C/X SAR in mountainous regions. *Remote Sensing of Environment*, **59**, 294–307.

Shi J. and Dozier J. (2000) Estimation of snow water equivalence using SIR-C/X SAR, Part I: inferring snow density and subsurface properties. *IEEE Journal of Geoscience and Remote Sensing*, **38**(6), 2465–2474.

Shi J., Dozier J. and Rott H. (1994) Snow mapping in alpine regions with synthetic aperture radar. *IEEE Journal of Geoscience and Remote Sensing*, **32**(1), 152–158.

Simpson J.J. and McIntire T.J. (2001) A recurrent neural network classifier for improved retrievals of areal extent of snow cover. *IEEE Transactions on Geoscience and Remote Sensing*, **39**(10), 2135–2147.

Singer F.S. and Popham R.W. (1963) Non-meteorological observations from weather satellites. *Astronautics and Aerospace Engineering*, **1**(3), 89–92.

Standley A.P. and Barrett E.C. (1999) The use of coincident DMSP SSM/I and OLS satellite data to improve snow cover detection and discrimination. *International Journal of Remote Sensing*, **20**(2), 285–305.

Steffen K. (1987) Bidirectional reflectance of snow at 500–600 nm. In *Large-Scale Effects of Seasonal Snow Cover*, Proceedings of the Vancouver Symposium, August 1987, Goodison B. (Ed.), IAHS: Vancouver, pp. 415–425.

Stiles W.H. and Ulaby F.T. (1980) The active and passive microwave response to snow parameters – 1. Wetness. *Journal of Geophysical Research*, **85**(C2), 1037–1044.

Stiles W.H., Ulaby F.T. and Rango A. (1981) Microwave measurements of snowpack properties. *Nordic Hydrology*, **12**, 143–166.

Stroeve J., Nolin A. and Steffen K. (1997) Comparison of AVHRR-derived and in situ surface albedo over the Greenland Ice sheet. *Remote Sensing of Environment*, **62**, 262–276.

Sturm M. and Benson C.S. (1997) Vapor transport, grain growth and depth hoar development in the subarctic snow. *Journal of Glaciology*, **43**(143), 42–59.

Sturm M., Holmgren J. and Liston G.E. (1995) A seasonal snow cover classification system for local to global applications. *Journal of Climatology*, **8**(5), 1261–1283.

Tait A.B., Barton J. and Hall D.K. (2001) A prototype MODIS-SSM/I snow mapping method. *Proceedings of a Symposium on Remote Sensing and Hydrology 2000*, April 2000, IAHS Publication No. 267: Santa Fe, pp. 139–144.

Tait A.B., Hall D.K., Foster J.L. and Armstrong R.L. (2000) Utilizing multiple datasets for snow-cover mapping. *Remote Sensing of Environment*, **72**, 111–126.

Tiuri M. and Hallikainen M. (1981) Microwave emission characteristics of snow covered earth surfaces measured by the Nimbus-7 satellite. *11th European Microwave Conference*, Amsterdam, September 7–11, 1981.

Trabant D. and Benson C. (1972) Field experiments on the development of depth hoar. *Studies in Mineralogy and Precambrian Geology*, Doe B.R. and Smith K.K. (Eds.), Geological Society of America Memoir 135: pp. 309–322.

Tsang L., Chen C.T., Chang A.T.C., Guo J. and Ding K.H. (2000) Dense media transfer theory based on quasicrystalline approximation with application to passive microwave remote sensing of new snow. *Radio Science*, **35**(3), 731–749.

Tsang L. and Kong J.A. (2001) *Scattering of Electromagnetic Waves: Advanced Topics*, John Wiley & Sons: New York.

Ulaby F.T., Moore R.K. and Fung A.K. (1986) *Microwave Remote Sensing, Active and Passive*, From *Theory to Applications*, Vol. 3, Addison-Wesley Publishing Company: Reading, p. 2162.

Ulaby F.T. and Stiles W.H. (1980) The active and passive microwave response to snow parameters 2. water equivalent of dry snow. *Journal of Geophysical Research*, **85**(C2), 1045–1049.

Ulaby F.T. and Stiles W.H. (1981) Microwave response of snow. *Advanced Space Research*, **1**, 131–149.

Ulaby F.T., Stiles W.H., Dellwig L.F. and Hanson B.C. (1977) Experiments on the radar backscatter of snow. *IEEE Transactions on Geoscience Electronics*, **GE-15**(4), 185–189.

Vikhamer D. and Solberg R. (2002) Subpixel mapping of snow cover in forests by optical remote sensing. *Remote Sensing of Environment*, **84**, 69–82.

Waite W.P. and MacDonald H.C. (1970) Snowfield mapping with K-band radar. *Remote Sensing of Environment*, **1**, 143–150.

Walker A.E. and Goodison B.E. (1993) Discrimination of a wet snow cover using passive-microwave satellite data. *Annals of Glaciology*, **17**, 307–311.

Walker A.E. and Goodison B. (2000) Challenges in determining snow water equivalent over Canada using microwave radiometry. *Proceedings of IGARSS 2000*, Honolulu, 24–28 July 2000.

Walker A.E. and Silis A. (2002) Snow-cover variations over the MacKenzie River Basin, Canada, derived from SSM/I passive-microwave satellite data. *Annals of Glaciology*, **34**, 8–14.

Warren S.G. (1982) Optical properties of snow. *Reviews of Geophysics and Space Physics*, **20**(1), 67–89.

Warren S.G. and Wiscombe W.J. (1980) A model for the spectral albedo of snow, II: snow containing atmospheric aerosols. *Journal of the Atmospheric Sciences*, **37**, 2734–2745.

Wergin W.P., Rango A., Erbe E.F. and Murphy C. (1996) Low temperature SEM of precipitated and metamorphosed snow crystals collected and transported from remote sites. *Journal of Microscopy Society of America*, **2**(3), 99–112.

Wergin W.P., Rango A., Foster J.L., Erbe E.F. and Pooley C. (2002) Irregular snow crystals: structural features as revealed by low temperature scanning electron microscopy. *Scanning*, **24**, 249–256.

Winther J.-G. (1993) Landsat TM-derived and in situ summer reflectance of glaciers in Svalbard. *Polar Research*, **12**(1), 37–55.

Winther J-G., Gerland S., Orbaek J.B., Ivanov B., Blanco A. and Boike J. (1999) *Hydrological Processes*, **13**, 2033–2049.

Wiscombe W.J. and Warren S.G. (1980) A model for the spectral albedo of snow, I. Pure snow. *Journal of the Atmospheric Sciences*, **37**, 2712–2733.